

Large-Area Super-Resolution 3D Digital Maps for Indoor and Outdoor Wireless Channel Modeling

Qianyu Zhang, Guanchong Niu, Man-On Pun
The Chinese University of Hong Kong, Shenzhen
Shenzhen, Guangdong, China, 518172

Abstract—This paper reports our recent work on creating the world’s first super-resolution 3D digital maps for indoor and outdoor wireless channel modeling. By exploiting the recent technological breakthroughs in unmanned aerial vehicle (UAV), Light Detection and Ranging (LiDAR) and the Simultaneous Localization and Mapping (SLAM) technology, this work develops a surveying system prototype to produce super-resolution 3D digital maps of centimeter-level resolution for large areas covering both indoor and outdoor environments. In addition, the resulting maps are designed to precisely capture building shapes even for skyscrapers with wall material information. It is believed that these new maps can potentially revolutionize the network planning practice commonly performed in the telecommunication industry by providing highly accurate indoor and outdoor channel models. By exploiting these new channel models, wireless service operators will be able to better optimize their wireless networks with reduced necessity of labor-intensive drive tests.

I. INTRODUCTION

The success of wireless communication systems such as WiFi or cellular networks has greatly transformed many aspects of our lives. However, one of the most critical challenges in deploying such wireless communication systems and the emerging fifth generation wireless systems (5G) is to provide good signal coverage, i.e. to provide strong wireless signal strength to support reliable voice/data communications over the whole service area. Fig. 1 shows the signal coverage for a hypothetical market with the red color indicating stronger signal strength while blue weaker signal strength.



Fig. 1. Wireless signal coverage prediction using 3D digital maps.

Clearly, bad signal coverage will incur low-quality wireless services such as call drops, resulting in poor customer satisfaction. Thus, it is very important for both wireless service providers and equipment vendors to ensure good signal coverage over the whole service area without coverage holes. In practice, this important engineering task is commonly achieved in a few standard steps, starting from network planning followed by field measurements and finally, network configuration optimization. More specifically, in the first step of network planning, signal coverage over the targeted service area is predicted by running computer simulation using either proprietary or commercial ray-tracing (such as Volcano from Siradel, France) software packages as shown in Fig. 2.

In addition to system parameters including transmitter locations and antenna configuration, the most important input to the ray-tracing software is the geodata, also commonly known as the high-resolution three-dimensional (HR 3D) digital map of the targeted service area. The prediction results are then inspected by experienced network engineers to ensure all minimum coverage requirements are satisfactorily met. If not, system parameters are optimized automatically and/or manually, including adjusting the transmission angles of base stations or even adding new base stations, before the signal coverage prediction is updated. This process is repeated until all minimum coverage requirements are satisfied.

The above computer-based network planning task has become the standard practice in the telecommunication industry nowadays. Despite its popularity, this approach is handicapped by two drawbacks. First, even empowered by the state-of-the-art ray-tracing technology that can model reflection and refraction phenomena accurately, the ray-tracing software remains incapable of capturing the scattering effects and depolarization process of the wireless channel. This drawback was *not* particularly detrimental for the pre-5G wireless systems operating in the sub-6GHz spectrum as their wireless channel is mostly dominated by dispersion impairments caused by reflections and refractions. In contrast, the other drawback related to the HR 3D digital map impacts the quality of the network planning for both current and future 5G systems. Originally generated from satellite imagery, most existing 3D digital maps have become rather obsolete in meeting the increasing demands for more sophisticated network planning. First, the existing maps do not cover indoor environments as satellites cannot see through the roofs and walls from the sky. As a result, the current network planning software can only provide rather

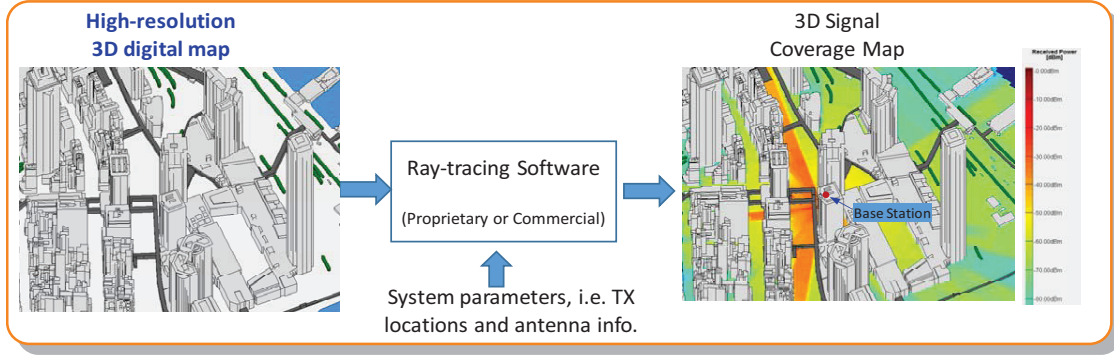


Fig. 2. Typical work flow for network planning using computer simulation.

inaccurate estimates for indoor coverage by extrapolating the outdoor signal coverage into indoor using a pre-determined penetration-plus-pathloss model without taking into account the wall and indoor structures (such as interior walls and doors and so on). In particular, since the wall material is unknown in the existing maps, all wall penetration losses are modeled using the same penetration loss model, regardless of the wall material and thickness. However, as reported in the literature [1], the penetration loss for different wall materials can vary substantially, e.g. the typical penetration loss for concrete walls is about 15 – 30dB while glass walls 3dB. Second, as shown in Fig. 2, all buildings are simply modeled as polygonal cylinders in the existing maps due to the fact that the aerial viewpoint from the satellite is obstructed by the building roofs. Therefore, even for buildings with extended roofs such as the famous Space Needle in Seattle, WA, the existing maps will simply model such buildings as polygonal cylinders, which clearly is erroneous. With the erroneous building shapes and missing information on the wall material and indoor structure, the indoor signal coverage provided by the existing maps is often rather poor and largely deviates from field measurements. Unfortunately, indoor signal coverage is very, if not the most, important, in network planning as majority of mobile users reside in indoor environments such as shopping malls. Finally, the finest digital maps currently available in the market are of two-meter resolution and generally rather expensive. A typical two-meter-resolution 3D digital map over a 1km-by-1km metropolitan area (such as the Vancouver downtown area) typically costs thousands of dollars. As a result, map vendors are very reluctant to produce maps for less popular markets. In the recent years, some attempts have been made to improve the indoor 3D maps by modeling a smaller conference room or music hall [2]. However, to the authors' best knowledge, most these maps are restricted to single indoor structure with very limited coverage.

In this project, we design and implement a surveying system prototype by exploiting the latest technological breakthroughs in unmanned aerial vehicle (UAV), Light Detection and Ranging (LiDAR) and the Simultaneous Localization and Mapping (SLAM) algorithm from the research field of robotics. The

resulting 3D digital maps can achieve super resolution on the order of a few centimeters, covering large-area indoor and outdoor environments. In addition, our maps can accurately capture the building shapes even for skyscrapers with wall material information at a much lower cost. The resulting maps can be easily utilized by any existing ray-tracing software with modification to generate highly accurate signal coverage maps over both indoor and outdoor environments. These new maps can potentially revolutionize the network planning doctrines currently practised by all wireless services operators by providing accurate indoor and outdoor channel models. This will subsequently enable operators to better optimize their wireless networks while reducing the necessity of labor-intensive drive tests.

II. PROPOSED SURVEYING SYSTEM



Fig. 3. Illustration of our surveying system prototype design

Taking advantages of recent technological advances in UAV and LiDAR, we propose a surveying system shown in Fig. 3. In this section, we will elaborate on each key component in the system.

A. LiDAR

Fig. 4 shows the VLP-16 LiDAR from Velodyne Acoustics, Inc employed in our system. The LiDAR is armed with 16 laser/detector pairs with effective detection range up to 100m with accuracy of $\pm 3\text{cm}$. Furthermore, the LiDAR is capable of transmitting 300,000 points per second, covering 30° of

vertical field of view (FOV) and 360° horizontal FOV. With 16 laser/detector pairs, the LiDAR boasts a vertical sampling resolution of about 2° , *i.e.* $[-15^\circ, -13^\circ, \dots, 13^\circ, 15^\circ]$.

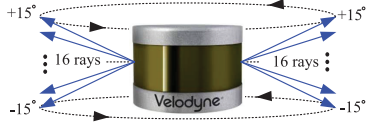


Fig. 4. VLP-16 LiDAR from Velodyne Acoustics, Inc.

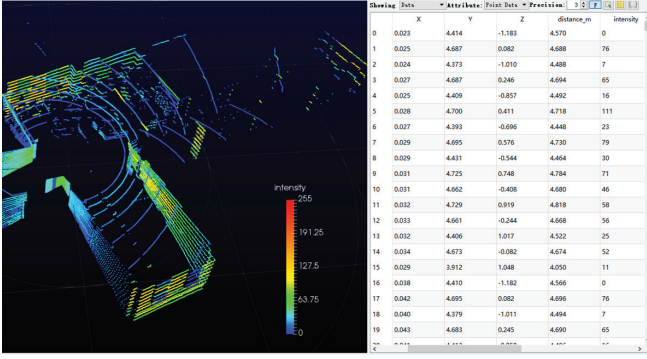


Fig. 5. Typical data collected from LiDAR.

In addition to the relative position (x, y, z) and distance of the detected object, each LiDAR data point also contains a field called intensity or calibrated reflectivity as shown in Fig. 5. The intensity measures the reflected power from the detected object. More specifically, the LiDAR is calibrated by Velodyne to generate an intensity value of 0 for absorbent diffuse reflectors while 101 for a semi-transparent white surface. As a result, a metal reflector will return a higher intensity value while glass 0. By inspecting the intensity of each data point, we can estimate the detected object's material.

The following table summarizes some of the key attributes of VLP-16. It is worth noting that the wavelength of the LiDAR falls within the infrared range. To avoid interference from pedestrians' body heat, our measurement experiments were mostly conducted during off-peak hours. Furthermore, despite VLP-16's compact size as compared to other LiDAR models in the market, the payload on UAV is mostly dominated by VLP-16's weight.

Attributes	Values
Horizontal/Vertical FOV	$360^\circ/30^\circ$
Rotational speed	5–20 rotations per second
Horizontal/Azimuth angular resolution	$0.1^\circ - 0.4^\circ$
Wavelength	903 nm
Power Consumption	8 W (Typical)
Weight	830g

B. UAV

In sharp contrast to the conventional drive test that loads all measurement equipment onto a ground vehicle, we propose to

mount the LiDAR at the bottom of a smaller quadcopter UAV such as the Phantom 4 pro model from DJI. Equipped with the latest UAV technology, such smaller quadcopter UAVs can easily navigate through outdoor and indoor environments. For instance, the Phantom 4 pro model from DJI considered in our system design has a diagonal size of about 350mm, which allows it to fly through regular hallways inside our teaching buildings on campus. In addition, such UAVs can also fly at a maximum speed of 72km per hour and maximum altitude of 500m, which enables the proposed surveying system to efficiently conduct throughout measurements over a larger metropolitan area. However, as a tradeoff for the smaller footprint, the Phantom 4 pro has a limited payload capacity. The UAV will become less stable if the payload exceeds 1kg. To fully utilize the UAV payload capacity, we propose to replace the camera originally installed at the bottom of the UAV with LiDAR as the camera is not used in our measurement in the current design yet. In particular, we propose to mount the LiDAR at a tilted angle as shown in Fig. 3. As shown Fig. 6, this tilted design allows the LiDAR to operate without being obstructed by the UAV body. Since the UAV moves back and forth to scan the measurement site in multiple passes, the entire site including the ceilings inside buildings can be thoroughly scanned.

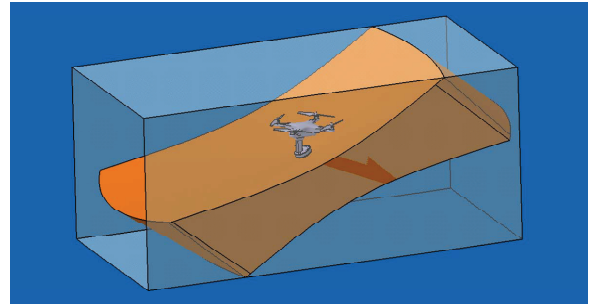


Fig. 6. Tilted design to scan without blind spots.

C. Data integration via SLAM

After collecting LiDAR measurement data, we then perform data integration to generate one unified SR 3D digital map for the measurement site. Since Global Position System (GPS) can be utilized to position each outdoor data point, outdoor data can be integrated in a more straightforward manner. In particular, we propose to utilize the differential GPS using Real Time Kinematic (RTK) that can significantly improve the real-time 3D positioning accuracy to the order of centimeters by measuring carrier phase difference between GPS user receiver and its GPS reference receiver [3]. In contrast, the integration of indoor data requires more sophisticated signal processing techniques as GPS is usually unavailable inside buildings. In our work, we propose to utilize the SLAM algorithm from the research areas in robotics to fuse the indoor and outdoor data together. SLAM was originally developed to enable mobile robots to autonomously navigate itself through an unfamiliar

environment. By extracting and matching feature points in the detected data, SLAM can simultaneously localize the robot's position and map out the surrounding environments [4].

More specifically, denoted by \mathbf{x}_k and \mathbf{u}_k the robot's position vector and the control vector applied to the robot at the time instant k , respectively, the history of the robot's locations and control vectors over all times k are given by

$$\mathbf{X}_{0:k} = \{\mathbf{x}_0, \mathbf{x}_1, \dots, \mathbf{x}_k\} = \{\mathbf{X}_{0:k-1}, \mathbf{x}_k\} \quad (1)$$

$$\mathbf{U}_{0:k} = \{\mathbf{u}_0, \mathbf{u}_1, \dots, \mathbf{u}_k\} = \{\mathbf{U}_{0:k-1}, \mathbf{u}_k\}. \quad (2)$$

For mapping purposes, the robot also keeps tracking N stationary landmarks (also commonly known as feature points) in the environments. Denoted by \mathbf{m} and \mathbf{z} the sets of the true and observed positions of all N landmarks, respectively, we have

$$\mathbf{m} = \{\mathbf{m}_0, \mathbf{m}_1, \dots, \mathbf{m}_N\}, \quad (3)$$

$$\mathbf{Z}_{0:k} = \{\mathbf{z}_0, \mathbf{z}_1, \dots, \mathbf{z}_k\} = \{\mathbf{Z}_{0:k-1}, \mathbf{z}_k\}, \quad (4)$$

where \mathbf{m}_n is the n -th landmark's position vector for $n = 1, 2, \dots, N$ while \mathbf{z}_k is the observation of \mathbf{m} at the time instant k .

The SLAM algorithm is designed to estimate the robot's current location \mathbf{x}_k and the map \mathbf{m} simultaneously in a probabilistic manner. More specifically, the problem can be formulated as sequential and iterative updates of the conditional probability of the map, *i.e.* $P(\mathbf{m}|\mathbf{X}_{0:k}, \mathbf{Z}_{0:k}, \mathbf{U}_{0:k})$ and the conditional probability of the robot's location, *i.e.* $P(\mathbf{x}_k|\mathbf{Z}_{0:k}, \mathbf{U}_{0:k}, \mathbf{m})$. These updates can be efficiently implemented via either the extended Kalman filter (EKF) or the Rao-Blackwellized particle filter [4]. It should be emphasized that GPS information is not required by SLAM as it tracks landmarks based on the characteristics of the environment. As a result, the output of the SLAM algorithm can provide very accurate relative distance between any two measurement data points without the knowledge of the *absolute* latitude and longitude coordinates of each data point. To label each data point with its *absolute* latitude and longitude coordinates, we can utilize some outdoor data points with detailed GPS information as anchor points. By exploiting these anchor points and the relative distance provided by SLAM, we can derive the latitude and longitude coordinates of each measurement data point in a straightforward manner.

III. MEASUREMENT RESULTS

To verify our design illustrated in Fig. 3, we developed a system prototype as shown in Fig. 7 to prove our design concept. For safety concerns, we have mounted the LiDAR on a pole fixed on a pushing cart in lieu of attaching the LiDAR onto a UAV as in the original design. Since both the height and tilt angle of the LiDAR can be adjusted along the pole, the design in Fig. 7 can reasonably mimic the operation of a LiDAR-bearing UAV without the risk of UAV crashes. Furthermore, the LiDAR is directly connected to a personal laptop running software package from Velodyne to collect LiDAR data before the data is processed by SLAM.

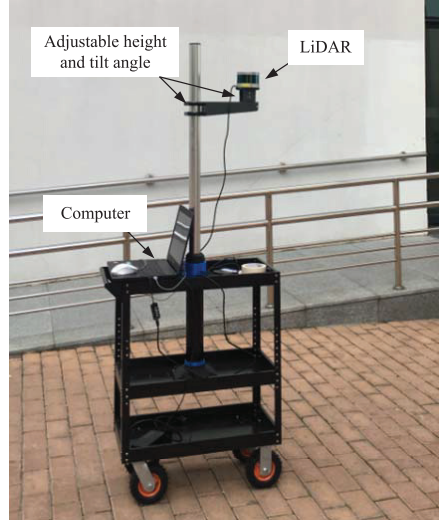


Fig. 7. Measurement system prototype developed for proof of concept.

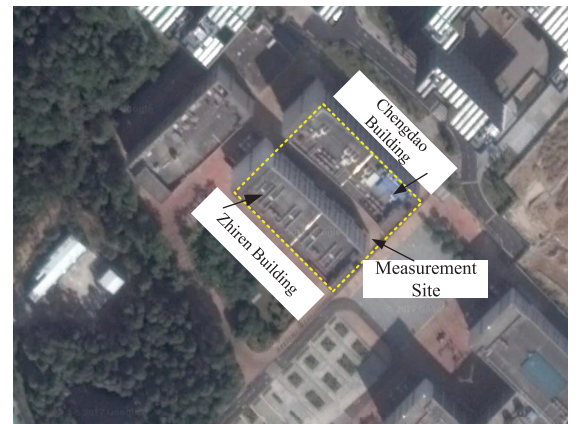


Fig. 8. Satellite image of the measurement site (Source: Google Earth).

Using the system prototype shown in Fig. 7, we performed extensive measurements on our campus shown in Fig. 8. The measurement site contains two six-floor buildings, namely the Zhiren Building and Chengdao Building. The two buildings each of which covers a ground area of $60 \times 20m^2$ are separated by 13m-wide open space. As shown in Fig. 8, the satellite image of the measurement site has rather limited resolution on the building structure and lacks of information on the indoor environment.

Fig. 9 shows the north-facing street view of the Zhiren Building captured in the open space between the two measurement buildings. As evidenced in Fig. 9, the wall of the Zhiren Building is featured with large glass windows on each floor. In particular, there is a $10 \times 1.5m$ bike shed attached to the Zhiren Building on the ground level. This bike shed is covered by a glass platform supported by a metal frame. Since the satellite imagery cannot distinguish such a glass platform from a regular concrete building structure, the conventional digital map may regard the bike shed as a smaller rectangular

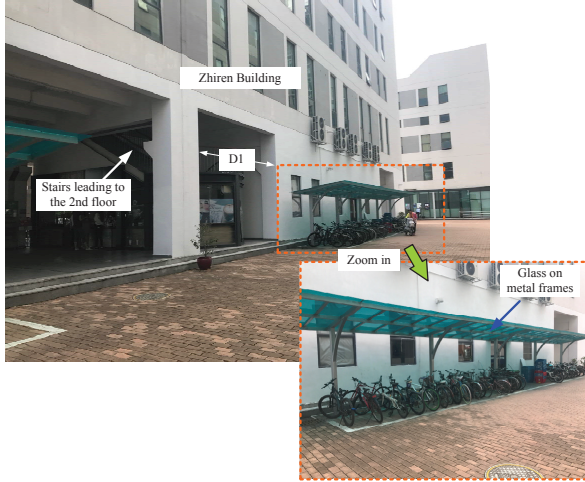


Fig. 9. North-facing street view of the Zhiren Building.

annex extending from the wall.



Fig. 10. North-facing street view of the Chengdao Building.

Fig. 10 shows the north-facing street view of the Chengdao Building. Similar to the Zhiren Building, the wall of Chengdao is also featured with large windows. Furthermore, a glass platform supported by metal frames extends from the wall at the height of about 3m above the ground. Again, satellite imagery will fail to characterize such a platform only based on the aerial view captured in the sky.

Next, we will demonstrate our measurement results by presenting the 3D models generated by SLAM. In the prototype, an improved SLAM algorithm called LiDAR Odometry and Mapping (LOAM) proposed in [5] has been adopted to integrate our indoor and outdoor measurement data. We first focus on the outdoor scenarios. As depicted in Fig. 11, since the glass generates very weak reflection, the LiDAR was able to accurately detect all glass windows and glass platform in the measurement site. It is worth noting that the colors in Fig. 11 are determined by the material of the reflector (glass, concrete or metal etc.) as well as the reflection angles. As a result, the colors of the metal frames for the bike shed attached to the

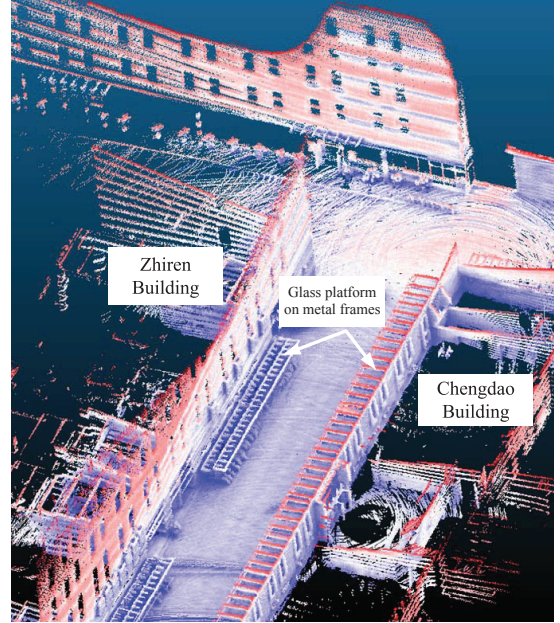


Fig. 11. Preliminary results on the outdoor measurements.

Zhiren Building and the glass platform installed on the wall of the Chengdao Building are slightly different, though they can be clearly differentiated from the glass windows.



Fig. 12. Indoor environment of the second floor of the Zhiren Building.

Next, we examine the indoor-outdoor measurement results. After data integration via LOAM, we then slice open the 3D building model and inspect different layers of the interior model. Using the second floor of the Zhiren Building shown in Fig. 12 as an example, we investigate the resulting 3D model shown in Fig. 13.

Inspection of Fig. 13 confirms that the resulting 3D model has successfully captured detailed information of the indoor environment of the Zhiren Building. It is worth noting that every indoor data point can be precisely positioned in terms of latitude and longitude by exploiting the outdoor anchor points, *e.g.* the bike shed data points shown at the bottom

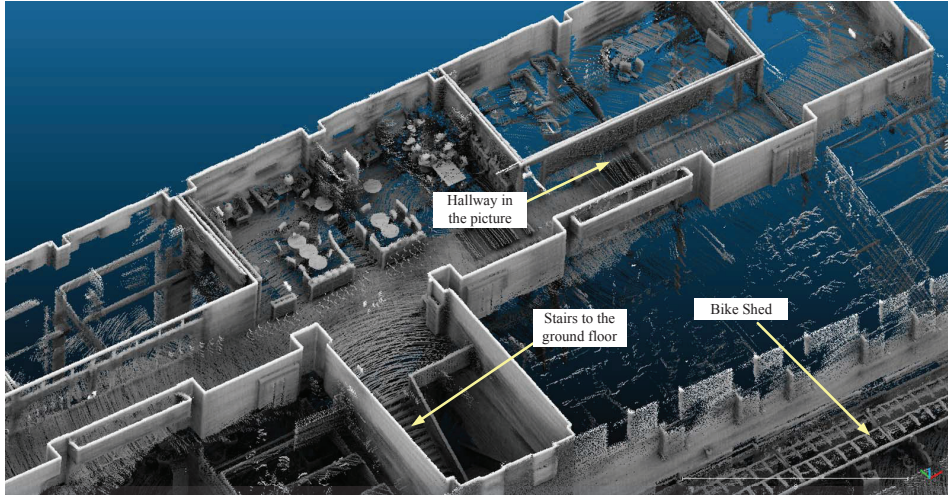


Fig. 13. Indoor-outdoor measurement results for the Zhiren Building.

right corner of Fig. 13. Furthermore, our 3D model provides much more detailed information than what may be required for wireless channel modeling. More specifically, for the purposes of wireless channel modeling, information on the wall materials (such as glass or concrete) and interior structure (such as positions of walls and doors) plays a very critical role while information on the indoor furniture is of less importance, though the additional information can be utilized for more detailed channel modeling purposes in the future.

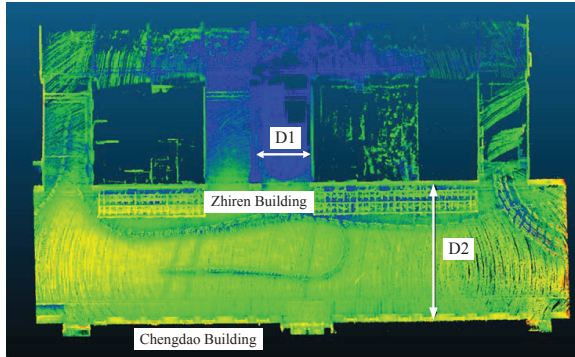


Fig. 14. Block diagram of the measurement system under consideration.

Finally, we investigate the accuracy of the resulting 3D models. We first identified some landmarks in the measurement site. After that, we compared the distance derived from our models and the actual measurement taken from a laser distance meter with millimeter-level accuracy. Fig. 14 shows two landmarks we used in this investigation, namely **D1**: the width of the stairs leading to the second floor in the Zhiren Building (also shown in Fig. 9) and **D2**: the distance between the Zhiren Building and Chengdao Building. The following table compares the distance measured for the two landmarks above. Clearly, our system prototype can achieve accuracy on the order of centimeters, which is consistent with the accuracy

of our LiDAR, GPS and the SLAM algorithm.

	D1 (m)	D2 (m)
Laser distance meter	13.026	5.886
Our results	13.064	5.868
Accuracy	99.7%	99.7%

IV. CONCLUSION

This paper has reported our recent work on developing a UAV-based surveying system empowered by the latest technological breakthroughs in LiDAR, UAV and SLAM technology. To prove our conceptual design, we have implemented a simplified system prototype and conducted extensive indoor and outdoor measurements on our campus. Based on our preliminary results, we have confirmed the feasibility of our design. The resulting super-resolution 3D digital maps are significantly superior to any existing digital maps used in wireless channel modeling as they achieve centimeter-level accuracy for both indoor and outdoor environments with wall material information. Such maps will be indispensable for future 5G deployment as most mobile users reside inside buildings. Future works include the development of a system prototype as depicted in Fig. 3, improvement on the 3D SLAM algorithm and further investigation on the wall penetration loss based on the reflectivity derived from LiDAR.

REFERENCES

- [1] R. Theodore, *Wireless Communications: Principles and Practice*. Upper Saddle River, NJ: Prentice Hall, 2002.
- [2] L. Faramondi, F. Inderst, S. Panzieri, and F. Pascucci, "Hybrid map building for personal indoor navigation systems," in *Proc. IEEE/ASME International Conference on Advanced Intelligent Mechatronics*, Besancon, France, July 2014, pp. 646–651.
- [3] Misra and Pratap, *Global Positioning System: signals, measurements, and performance*. Ganga-Jamuna Press, 2011.
- [4] D.-W. Hugh and T. Bailey, "Simultaneous localization and mapping: Part I," *IEEE International Conference on Robotics and Automation (ICRA)*, vol. 13, no. 2, pp. 99–110, 2006.
- [5] J. Zhang and S. Singh, "LOAM: Lidar odometry and mapping in real-time," in *Proc. IEEE Robotics: Science and Systems Conference (RSS)'15*, Seattle, WA, USA, 2015, pp. 2174–2181.